

4. PRODUCTION AND PROPERTIES OF RADIATIONS

the decrease in amplitude of the wave, and $\text{Im}[-\varepsilon^{-1}(\omega)]$ is related to the energy loss of a fast electron. The above curve shows some exchange of oscillator strength from core to valence electrons, arising from the Pauli principle, which forbids transitions to occupied states for the deeper electrons.

More practically, in the microanalytical domain, the combination of high performance attained by using EELS with parallel detection (*i.e.* energy resolution below 1 eV, spatial resolution below 1 nm, minimum concentration below 10^{-3} atom, time resolution below 10 ms) makes it a unique tool for studying local electronic properties in solid specimens.

4.3.5. Oriented texture patterns (By B. B. Zvyagin)

4.3.5.1. Texture patterns

The formation of textures in specimens for diffraction experiments is a natural consequence of the tendency for crystals of a highly anisotropic shape to deposit with a preferred orientation. The corresponding diffraction patterns may present some special advantages for the solution of problems of phase and structure analysis. Lamellar textures composed of crystals with the most fully developed face parallel to a plane but randomly rotated about its normal are specially important. The ease of interpretation of patterns of such textures when oriented obliquely to the primary beam (*OT* patterns) is a valuable property of the electron-diffraction method (Pinsker, 1953; Vainshtein, 1964; Zvyagin, 1967; Zvyagin, Vrublevskaya, Zhukhlistov, Sidorenko, Soboleva & Fedotov, 1979). Texture patterns (*T* patterns) are also useful in X-ray diffraction (Krinary, 1975; Mamy & Gaultier, 1976; Plançon, Rousseaux, Tchoubar, Tchoubar, Krinari & Drits, 1982).

4.3.5.2. Lattice plane oriented perpendicular to a direction (lamellar texture)

If in the plane of orientation (the texture basis) the crystal has a two-dimensional cell a, b, γ , the c^* axis of the reciprocal cell will be the texture axis. Reciprocal-lattice rods parallel to c^* intersect the plane normal to them (the ab plane of the direct lattice) in the positions hk of a two-dimensional net that has periods $1/a \sin \gamma$ and $1/b \sin \gamma$ with an angle $\gamma' = \pi - \gamma$ between them, whatever the direction of the c axis in the direct lattice.

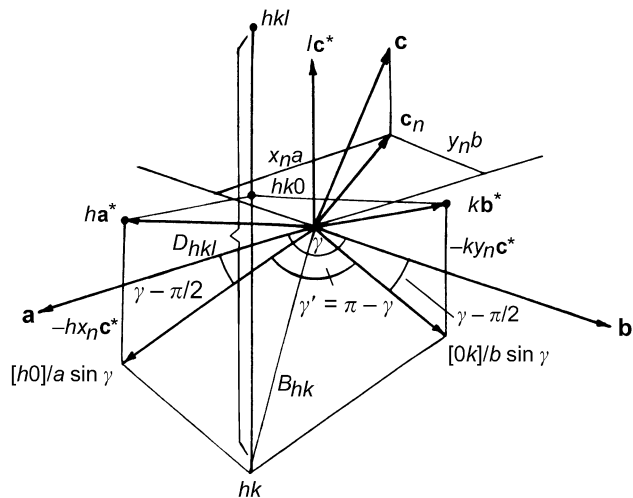


Fig. 4.3.5.1. The relative orientations of the direct and the reciprocal axes and their projections on the plane ab , with indication of the distances B_{hk} and D_{hkl} that define the positions of reflections in lamellar texture patterns.

The latter is defined by the absolute value c and the normal projection c_n on the ab plane, with components x_n, y_n along the axes a, b . In the triclinic case,

$$x_n = (c/a)(\cos \beta - \cos \alpha \cos \gamma) / \sin^2 \gamma \quad (4.3.5.1)$$

$$y_n = (c/b)(\cos \alpha - \cos \beta \cos \gamma) / \sin^2 \gamma \quad (4.3.5.2)$$

(Zvyagin *et al.*, 1979). The lattice points of each rod with constant hk and integer l are at intervals of $c^* = 1/d_{001}$, but their real positions, described by their distances D_{hkl} from the plane ab , depend on the projections of the axes a^* and b^* on c^* (see Fig. 4.3.5.1), the equations

$$x_n = -a^* \cos \beta^* / c^* \quad (4.3.5.3)$$

$$y_n = -b^* \cos \alpha^* / c^* \quad (4.3.5.4)$$

being satisfied.

The reciprocal-space representation of a lamellar texture is formed by the rotation of the reciprocal lattice of a single crystal about the c^* axis. The rods hk become cylinders and the lattice points become circles lying on the cylinders. In the case of high-energy electron diffraction (HEED), the wavelength of the electrons is very short, and the Ewald sphere, of radius $1/\lambda$, is so great that it may be approximated by a plane passing through the origin of reciprocal space and normal to the incident beam. The patterns differ in their geometry, depending on the angle φ through which the specimen is tilted from perpendicularity to the primary beam. At $\varphi = 0$, the pattern consists of hk rings. When $\varphi \neq 0$ it contains a two-dimensional set of reflections hkl falling on hk ellipses formed by oblique sections of the hk cylinders. In the limiting case of $\varphi = \pi/2$, the ellipses degenerate into pairs of parallel straight lines theoretically containing the maximum numbers of reflections. The reflection positions are defined by two kinds of distances: (1) between the straight lines hk (length of the short axes of the ellipses hk):

$$B_{hk} = (1/\sin \gamma)(h^2/a^2 + k^2/b^2 - 2hk \cos \gamma/ab)^{1/2} \quad (4.3.5.5)$$

and (2) from the reflection hkl to the line of the short axes:

$$D_{hkl} = (ha^* \cos \beta^* / c^* + kb^* \cos \alpha^* / c^* + l)c^* \quad (4.3.5.6)$$

$$= (-hx_n - ky_n + l)/d_{001}. \quad (4.3.5.7)$$

In patterns obtained under real conditions ($0 < \varphi < \pi/2$, accelerating voltage V proportional to λ^{-2} , distance L between the specimen and the screen), these values are presented in the scale of $L\lambda$, D_{hkl} also being proportional to $1/\sin \varphi$ with maximum value $D_{\max} = B_{hk} \tan \varphi$ for the registrable reflections. The values of B_{hk} and D_{hkl} , determined by the unit cells and the indices hkl , are the objects of the geometrical analysis of the *OT* patterns. When the symmetry is higher than triclinic, the expression for B_{hk} and D_{hkl} are much simpler.

Such *OT* patterns are very informative, because the regular two-dimensional distribution of the hkl reflections permits definite indexing, cell determination, and intensity measurements. For low-symmetry and fine-grained substances, they present unique advantages for phase identification, polytypism studies, and structure analysis.

In the X-ray study of textures, it is impossible to neglect the curvature of the Ewald sphere and the number of reflections recorded is restricted to larger d values. However, there are advantages in that thicker specimens can be used and reflections with small values of B_{hk} , especially the $00l$ reflections, can be recorded. Such patterns are obtained in usual powder cameras with the incident beam parallel to the platelets of the oriented aggregate and are recorded on photographic film in the form of hkl reflection sequences along hk lines, as was demonstrated by

4.3. ELECTRON DIFFRACTION

Mamy & Gaultier (1976). The hk lines are no longer straight, but have the shapes described by Bernal (1926) for rotation photographs. It is difficult, however, to prepare good specimens. Other arrangements have been developed recently with advantages for precise intensity measurements. The reflections are recorded consecutively by means of a powder diffractometer fitted with a goniometer head. The relation between the angle of tilt φ and the angle of diffraction (twice the Bragg angle) 2θ depends on the reciprocal-lattice point to be recorded. If the latter is defined by a vector of length $H = (2 \sin \theta)/\lambda$ and by the angle ω between the vector and the plane of orientation (texture basis), the relation $\varphi = \theta - \omega$ permits scanning of reciprocal space along any trajectory by proper choice of consecutive values of ω or θ . In particular, if ω is constant, the trajectory is a straight line passing through the origin at an angle ω to the plane of orientation (Krinary, 1975). Using additional conditions [$\omega = \arctan(D/B)$, $H = (B^2 + D^2)^{1/2}$], Plançon *et al.* (1982) realized the recording and the measurement of intensities along the cylinder-generating hk rods for different shapes of the misorientation function $N(\alpha)$.

In the course of development of electron diffractometry, a deflecting system has been developed that permits scanning the electron diffraction pattern across the fixed detector along any direction over any interval (Fig. 4.3.5.2). The intensities are measured point by point in steps of variable length. This system

is applicable to any kind of two-dimensional intensity pattern, and in particular to texture patterns (Zvyagin, Zhukhlistov & Plotnikov, 1996). Electron diffractometry provides very precise intensity measurements and very reliable structural data (Zhukhlistov *et al.*, 1997).

If the effective thickness of the lamellae is very small, of the order of the lattice parameter c , the diffraction pattern generates into a combination of broad but recognizably distinct $00l$ reflections and broad asymmetrical hk bands (Warren, 1941). The classical treatments of the shape of the bands were given by Méring (1949) and Wilson (1949) [for an elementary introduction see Wilson (1962)].

4.3.5.3. Lattice direction oriented parallel to a direction (fibre texture)

A fibre texture occurs when the crystals forming the specimen have a single direction in common. Each point of the reciprocal lattice describes a circle lying in a plane normal to the texture axis. The pattern, considered as plane sections of the reciprocal-lattice representation, resembles rotation diagrams of single crystals and approximates to the patterns given by cylindrical lattices (characteristic, for example, of tubular crystals).

If the a axis is the texture axis, the hk rods are at distances

$$B_{hk} = (-h \cos \gamma/a + k/b)/\sin \gamma \quad (4.3.5.8)$$

from the texture axis and

$$D_{hk} = h/a \quad (4.3.5.9)$$

from the plane normal to the texture axis (the zero plane b^*c^*). On rotation, they intersect the plane normal to the incident beam and pass through the texture axis in layer lines at distances D_{hk} from the zero line, while the reflection positions along these lines are defined by their distances from the textures axis (see Fig. 4.3.5.3):

$$B_{hkl} = [B_{hk}^2 + (-hx_n - ky_n + l)^2/d_{001}^2]^{1/2}. \quad (4.3.5.10)$$

If the texture axis forms an angle ε with the a axis and $\delta = \varepsilon - \gamma + \pi/2$ with the projection of a^* on the plane ab , then

$$B_{hk} = \{-h(\sin \delta)/a + k[\sin(\gamma' - \delta)]/b\}/\sin \gamma \quad (4.3.5.11)$$

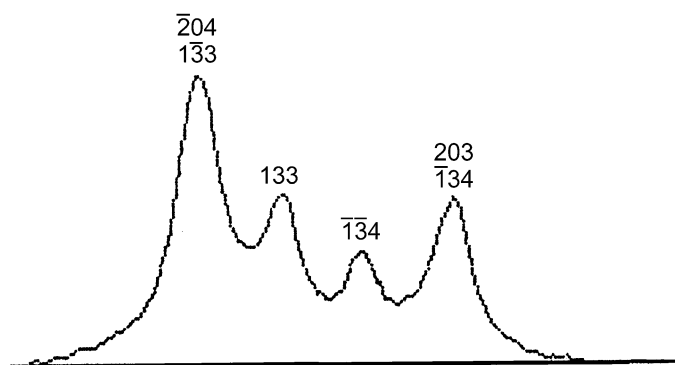
$$= \{-h[\cos(\gamma - \varepsilon)]/a + k \cos \varepsilon/b\}/\sin \gamma \quad (4.3.5.12)$$

$$D_{hk} = \{h(\cos \delta)/a + k[\cos(\gamma' - \delta)]/b\}/\sin \gamma \quad (4.3.5.13)$$

$$= \{h[\sin(\gamma - \varepsilon)]/a + k \sin \varepsilon/b\}/\sin \gamma. \quad (4.3.5.14)$$



(a)



(b)

Fig. 4.3.5.2. (a) Part of the OTED pattern of the clay mineral kaolinite and (b) the intensity profile of a characteristic quadruplet of reflections recorded with the electron diffractometry system. The scanning direction is indicated in (a).

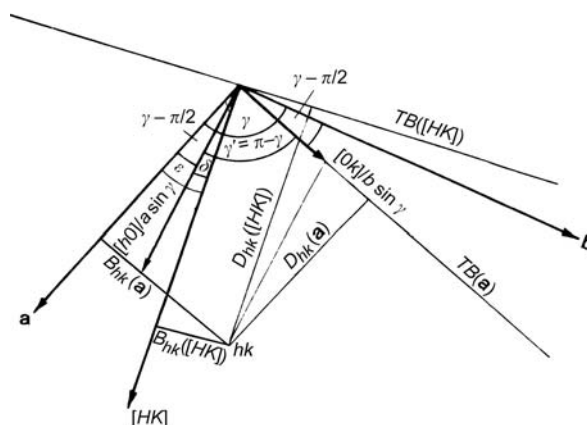


Fig. 4.3.5.3. The projections of the reciprocal axes on the plane ab of the direct lattice, with indications of the distances B and D of the hk rows from the fibre-texture axes a or $[hk]$.

4. PRODUCTION AND PROPERTIES OF RADIATIONS

The relation between the angles δ , ε , and the direction $[hk]$ of the texture axis is given by the expression

$$\begin{aligned}\cos \delta &= \sin(\gamma - \varepsilon) \\ &= [h/a - k(\cos \gamma)/b] \\ &\quad \times [h^2 a^{-2} + k^2 b^{-2} - 2hk(\cos \gamma)/ab]^{-1/2}. \quad (4.3.5.15)\end{aligned}$$

The layer lines with constant h that coincide when $\varepsilon = 0$ are split when $\varepsilon \neq 0$ according to the sign of k , since then $D_{hk} \neq D_{h\bar{k}}$ and B_{hk} and $B_{h\bar{k}}$ defining the reflection positions along the layer line take other values. Such peculiarities have been observed by means of selected-area electron diffraction for tabular particles and linear crystal aggregates of some phyllosilicates in the simple case of $\gamma = \pi/2$ (Gritsaenko, Zvyagin, Boyarskaya, Gorshkov, Samotoin & Frolova, 1969).

When fibres or linear aggregates are deposited on a film (for example, in specimens for high-resolution electron diffraction) with one direction parallel to a plane, they form a texture that is intermediate between lamellar and fibre. The points of the reciprocal lattice are subject to two rotations: around the fibre axis and around the normal to the plane. The first rotation results in circles, the second in spherical bands of different widths, depending on the position of the initial point relative to the texture axis and the zero plane normal to it. The diffraction patterns correspond to oblique plane sections of reciprocal space, and consist of arcs having intensity maxima near their ends; in some cases, the arcs close to form complete circles. In particular, when the particle elongation is in the a direction, the angular range of the arcs decreases with h and increases with k (Zvyagin, 1967).

4.3.5.4. Applications to metals and organic materials

The above treatment, though general, had layer silicates primarily in view. Texture studies are particularly important for metal specimens that have been subjected to cold work or other treatments; the phenomena and their interpretation occupy several chapters of the book by Barrett & Massalski (1980). Similarly, Kakudo & Kasai (1972) devote much space to texture in polymer specimens, and Guinier (1956) gives a good treatment of the whole subject. The mathematical methods for describing and analysing textures of all types have been described by Bunge (1982; the German edition of 1969 was revised in many places and a few errors were corrected for the English translation).

4.3.6. Computation of dynamical wave amplitudes

4.3.6.1. The multislice method (By D. F. Lynch)

The calculation of very large numbers of diffracted orders, *i.e.* more than 100 and often several thousand, requires the multislice procedure. This occurs because, for N diffracted orders, the multislice procedure involves the manipulation of arrays of size N , whereas the scattering matrix or the eigenvalue procedures involve manipulation of arrays of size N by N .

The simplest form of the multislice procedure presumes that the specimen is a parallel-sided plate. The surface normal is usually taken to be the z axis and the crystal structure axes are often chosen or transformed such that the c axis is parallel to z and the a and b axes are in the xy plane. This can often lead to rather unconventional choices for the unit-cell parameters. The maximum tilt of the incident beam from the surface normal is restricted to be of the order of 0.1 rad. For the calculation of wave amplitudes for larger tilts, the structure must be reprojected down an axis close to the incident-beam direction.

For simple calculations, other crystal shapes are generally treated by the column approximation, that is the crystal is presumed to consist of columns parallel to the z axis, each column of different height and tilt in order to approximate the desired shape and variation of orientation.

The numerical procedure involves calculation of the transmission function through a thin slice, calculation of the vacuum propagation between centres of neighbouring slices, followed by evaluation in a computer of the iterated equation

$$u_n(h, k) = p_n \{p_{n-1} \dots p_3 [p_2 (p_1 q_1 * q_2) * q_3] * \dots * q_n\} \quad (4.3.6.1)$$

in order to obtain the scattered wavefunction, $u_n(h, k)$, emitted from slice n , *i.e.* for crystal thickness $H = \Delta z_1 + \Delta z_2 + \dots + \Delta z_n$; the symbol $*$ indicates the operation 'convolution' defined by

$$f_1(x) * f_2(x) = \int_{-\infty}^{\infty} f_1(w) f_2(x - w) dw,$$

and

$$p_n = \exp(-i2\pi\Delta z_n(\lambda/2)\{[h(h-h'')/a^2] + [k(k-k'')/b^2]\})$$

is the propagation function in the small-angle approximation between slice $n-1$ and slice n over the slice spacing Δz_n . For simplicity, the equation is given for orthogonal axes and h'' , k'' are the usually non-integral intercepts of the Laue circle on the reciprocal-space axes in units of $(1/a)$, $(1/b)$. The excitation errors, $\zeta(h, k)$, can be evaluated using

$$\zeta(h, k) = -(\lambda/2)\{[h(h-h'')/a^2] + [k(k-k'')/b^2]\}. \quad (4.3.6.2)$$

The transmission function for slice n is

$$q_n(h, k) = F\{\exp[i\sigma\varphi_n(x, y)\Delta z_n]\}, \quad (4.3.6.3)$$

where F denotes Fourier transformation from real to reciprocal space, and

$$\varphi_n(x, y)\Delta z_n = {}^p\varphi(x, y) = \int_{z_{n-1}}^{z_{n-1}+\Delta z_n} \varphi(x, y, z) dz$$

and

$$\sigma = \frac{\pi}{W\lambda} \frac{2}{1 + (1 - \beta^2)^{1/2}}$$

and

$$\beta = \frac{v}{c},$$

where W is the beam voltage, v is the relativistic velocity of the electron, c is the velocity of light, and λ is the relativistic wavelength of the electron.

The operation $*$ in (4.3.6.1) is most effectively carried out for large N by the use of the convolution theorem of Fourier transformations. This efficiency presumes that there is available an efficient fast-Fourier-transform subroutine that is suitable for crystallographic computing, that is, that contains the usual crystallographic normalization factors and that can deal with a range of values for h , k that go from negative to positive. Then,

$$u_n(h, k) = F\{F^{-1}[u_{n-1}(h, k)]F^{-1}[q_n(h, k)]\}, \quad (4.3.6.4)$$

where F denotes

$$u(h, k) = \frac{1}{n_x n_y} \sum_{x=1}^{n_x} \sum_{y=1}^{n_y} U(x, y) \exp\left\{2\pi i \left[\frac{hx}{n_x}, \frac{ky}{n_y}\right]\right\}$$

and F^{-1} denotes